Improving the Robustness in Extracting 3D Point Landmarks from 3D Medical Images Using Parametric Deformable Models

Manfred Alker[1], Sönke Frantz[1], Karl Rohr[2], and H. Siegfried Stiehl[1]

[1] Universität Hamburg, FB Informatik, AB Kognitive Systeme, Vogt-Kölln-Str. 30, D-22527 Hamburg, {alker,frantz,stiehl}@kogs.informatik.uni-hamburg.de
[2] International University in Germany, D-76646 Bruchsal, rohr@i-u.de

Abstract. Existing approaches to the extraction of 3D point landmarks based on parametric deformable models suffer from their dependence on a good model initialization to avoid local suboptima during model fitting. Our main contribution to increasing the robustness of model fitting against local suboptima is a *novel hybrid optimization algorithm* combining the advantages of both the conjugate gradient (cg-)optimization method (known for its time efficiency) and genetic algorithms (exhibiting robustness against local suboptima). It has to be stressed, however, that the scope of applicability of this nonlinear optimization method is considered to be not restricted to model fitting problems in medical image analysis. We apply our model fitting algorithm to 3D medical images depicting tip-like and saddle-like anatomical structures such as the horns of the lateral ventricles in the human brain or the zygomatic bone as part of the skull. Experimental results for 3D MR and CT images demonstrate that in comparison to a purely local cg-optimization method, the robustness of model fitting in the case of poorly initialized model parameters is significantly improved with a hybrid optimization strategy. Moreover, we compare an *edge strength-based fitting measure* with an *edge distance-based fitting measure* w.r.t. their suitability for model fitting.

1 Introduction

The extraction of 3D anatomical point landmarks from 3D tomographic images is a prerequisite for landmark-based approaches to 3D image registration, which is a fundamental problem in computer-assisted neurosurgery. While earlier approaches to 3D point landmark extraction exploit the local characteristics of the image data by applying differential operators (e.g, [16],[11]), an approach based on parametric deformable models has recently been proposed in [5]. The approach in [5] takes into account more global image information than existing differential approaches, allows to localize 3D point landmarks more accurately, and also reduces the number of false detections. However, since a local optimization method is employed, a drawback of this approach is the need of a good model initialization in order to avoid local suboptima during model fitting.

For the purpose of increasing the robustness of model fitting in the case of poorly initialized model parameters, we propose a new *hybrid optimization algorithm* that is suitable for general poorly initialized nonlinear optimization

problems and that combines the computational efficiency of the (local) conjugate gradient (cg-)optimization method with the robustness of (global) genetic algorithms against local suboptima. Existing optimization algorithms for model fitting problems are either purely local (e.g., [13],[18],[1],[5]) or strictly global (e.g., [4],[17]). Moreover we compare an *edge strength-based fitting measure* based on the strength of the intensity gradient along the model surface (e.g., [18]) with an *edge distance-based fitting measure* (cf., e.g., [1]) w.r.t. their suitability for model fitting. The fitting algorithm proposed here is applied to the extraction of salient surface loci (curvature extrema) of *tip-* and *saddle-like structures* such as the ventricular horns in the human brain or the saddle points at the zygomatic bones being part of the skull (see Fig. 1(a),(b)). To represent the 3D shape

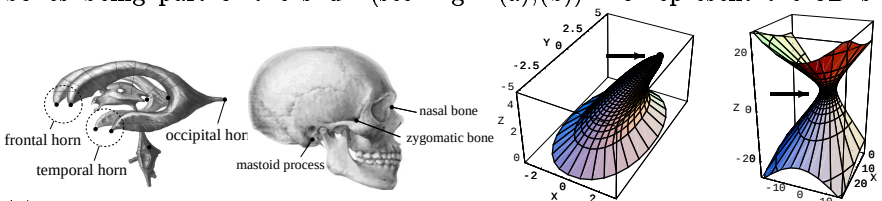

(a) (b) (c) (d)

Fig. 1. (a),(b): Ventricular horns of the human brain (from [12]) and the human skull (from [2]). Examples of 3D point landmarks are indicated by black dots. **(c),(d)**: Quadric surfaces as parametric deformable models for tips ((c): bended and tapered half-ellipsoid) and for saddle structures ((d): undeformed half-hyperboloid of one sheet). The landmark positions are indicated by a black dot.

of such structures, we utilize quadric surfaces undergoing global deformations (Sect. 2). The fitting measures for model fitting are then described in Sect. 3, while our hybrid algorithm for optimizing a fitting measure w.r.t. the model parameters is outlined in Sect. 4. Experimental results of studying the robustness of model fitting for 3D tomographic images of the human head are presented in Sect. 5. In particular, we analyze the landmark localization accuracy of our new approach and compare it with that of a purely local cg-optimization algorithm.

2 Modeling Tip- and Saddle-Like Structures with Quadrics

In the literature, a variety of 3D surface models has been used for different applications (e.g., [13],[15],[4],[18],[1]; see [9] for a survey). As geometric models for tip- and saddle-like structures, we here use quadric surfaces ([5]) since they well represent the anatomical structures of interest here, but still have few model parameters, and both a parametric and an implicit defining function. Bended and tapered ellipsoids are utilized for representing 3D tip-like structures such as the ventricular horns, whereas hyperboloids of one sheet are used for 3D saddle-like structures such as the zygomatic bones (see Fig. 1(c),(d)). For tip-like structures, the *parametric form* of our model is obtained by applying quadratic bending [4] and linear tapering deformations [13],[4] as well as a rigid transformation allowing for arbitrary poses in 3D space to the parametric form of an ellipsoid:

$$\boldsymbol{x}_{tip}(\theta,\phi) = \boldsymbol{R}_{\alpha,\beta,\gamma} \begin{pmatrix} a_1 \cos\theta \cos\phi/(\rho_x \sin\theta+1)+\delta\cos\upsilon(a_3\sin\theta)^2 \\ a_2 \cos\theta \sin\phi/(\rho_y \sin\theta+1)+\delta\sin\upsilon(a_3\sin\theta)^2 \\ a_3 \sin\theta \end{pmatrix} + \boldsymbol{t}, \qquad (1)$$

where $0 \leq \theta \leq \pi/2$ and $-\pi \leq \phi < \pi$ are the latitude and longitude angle parameters, resp. Further on, $a_1, a_2, a_3 > 0$ are scaling parameters, δ, υ determine the bending strength and direction, resp., and $\rho_x, \rho_y \geq 0$ determine the tapering strengths in x- and y-direction. For the rigid transformation, α, β, γ denote the Eulerian angles of rotation and $\boldsymbol{t}^T = (X, Y, Z)$ is the translation vector of the origin. Hence, the model is described by the parameter vector $\boldsymbol{p} = (a_1, a_2, a_3, \delta, \upsilon, \rho_x, \rho_y, X, Y, Z, \alpha, \beta, \gamma)$. The landmark position is then given by $\boldsymbol{x}_l = \boldsymbol{x}_{tip}(\pi/2, 0) = \boldsymbol{R}_{\alpha,\beta,\gamma}(\delta \cos \upsilon\, a_3^2, \delta \sin \upsilon\, a_3^2, a_3)^T + \boldsymbol{t}$. The *parametric form* of hyperboloids of one sheet is the same as the one given in [5].

3 Model Fitting with Edge-Based Fitting Measures

To fit the geometric models from Sect. 2 to the image data, a fitting measure is optimized w.r.t. the model parameters. Here, we consider an edge strength-based fitting measure and an edge distance-based fitting measure.

For the *edge strength-based fitting measure* M_{ES} (e.g., [18],[14]), the strength of the intensity gradient e_g is integrated over the model surface M:

$$M_{ES}(\boldsymbol{p}) = -\int_M e_g(\boldsymbol{x}) dF = -\iint_{\theta,\phi} e_g(\boldsymbol{x}(\theta,\phi)) \left\| \frac{\partial \boldsymbol{x}}{\partial \theta} \times \frac{\partial \boldsymbol{x}}{\partial \phi} \right\| d\theta d\phi \rightarrow \text{Min!}, \quad (2)$$

where $e_g(\boldsymbol{x}) = \|\boldsymbol{\nabla} g(\boldsymbol{x})\|$ is the gradient magnitude of the intensity function g and $\boldsymbol{x}$ is a point on the model surface M which is parameterized by θ, ϕ. To emphasize small surfaces, we additionally apply a *surface weighting factor* to the fitting measure (2) which then takes the form $M_{ES} = -\frac{\int_M e_g(\boldsymbol{x}) dF}{\sqrt{\int_M dF}}$.

The *edge distance-based fitting measure* M_{ED} used here is written as (cf., e.g., [13],[1],[17])

$$M_{ED}(\boldsymbol{p}) = \sum_{i=1}^{N} e_g(\boldsymbol{\xi}_i)\ \rho\left(\frac{1 - \hat{\mathrm{F}}(\boldsymbol{\xi}_i, \boldsymbol{p})}{\|\boldsymbol{\nabla} \hat{\mathrm{F}}(\boldsymbol{\xi}_i, \boldsymbol{p})\|} \right) \rightarrow \text{Min!}. \quad (3)$$

The sum is taken over all N image voxels $\boldsymbol{\Xi} = \{\boldsymbol{\xi}_1, \ldots, \boldsymbol{\xi}_N\}$ which – to diminish the influence of neighbouring structures – lie within a *region-of-interest (ROI)* and whose edge strength $e_g(\boldsymbol{\xi}_i)$ exceeds a certain threshold value. The vector of model parameters is denoted by $\boldsymbol{p}$. Further on, we use $\rho(x) = |x|^{1.2}$ for all $x \in \mathbb{R}$ as a distance weighting function to reduce the effect of outliers ([19]). The argument of ρ is a first order distance approximation between the image voxel with coordinates $\boldsymbol{\xi}_i$ and the model surface (cf., e.g., [17]). The inside-outside function of the tapered and bended quadric surface after applying a rigid transform is denoted by $\hat{\mathrm{F}}$ (cf., e.g., [13],[4],[1]). Also, a volume factor is used in conjunction with (3) to emphasize small volumes. This factor has been chosen as $1 + \frac{a_1 a_2 a_3}{a_{1,est} a_{2,est} a_{3,est}}$, where the weighting factor $a_{1,est} a_{2,est} a_{3,est}$ is coarsely estimated to a value of 10^3 voxel units (vox). For volume weighting factors (or size factors), see also, e.g., [13].

4 A Novel Hybrid Optimization Algorithm

Most optimization algorithms considered in the literature for fitting deformable models are local algorithms such as the *conjugate gradient (cg-)method* (e.g., [13],[18],[1],[5]). The cg-method combines problem specific search directions

of the *method of steepest descent* with optimality properties of the method of *conjugate directions* (e.g., [6]). However, since it is a purely local method, it is prone to run into local suboptima. On the other hand, global optimization methods such as genetic algorithms (GAs; e.g., [7]) have been proposed to avoid running into local suboptima (e.g., [4],[17]). However, global methods are plagued with slow convergence rates. We here propose a *hybrid algorithm* which combines the advantages of a local optimization method such as the cg-method (computational efficiency) with a global method similar to a GA (robustness against local suboptima). Similar to GAs, we consider a whole *population* of parameter vectors which all compete for finding the *global optimum*. However, there are several differing features of our approach to traditional GAs such as the *mutation strategy*, which in our case is much better motivated and adapted to the specific optimization problem. Traditional GAs use *bit-flips* and *crossovers* to imitate natural mutation strategies ([7]). By contrast, our search strategy is to use not only the global optimum resulting from the *line search algorithm* at the end of each cg-step, but several most promising local optima resulting from line search in order to obtain a new population of parameter vectors. The search strategy may either draw upon only a few population members – calculating many cg-iterations per member (in-depth-search) – or it may incorporate many population members. Depending on the particular optimization problem at hand, either the former or the latter strategy may show better convergence behaviour. Because we want to have one strategy which is able to cope with a broad class of optimization problems, we dynamically adapt the population size to the complexity of the problem by increasing the maximal population size each time a candidate solution converges to a local optimum, i.e. when its objective function value does not improve for a given number of cg-iterations. Consequently, several parameters can be adapted to the specific optimization problem at hand:

- the maximum population size that must not be exceeded (here: 20),
- the number of cg-iterations after which the least successful population members (measured by their objective function values) are discarded (here: 5),
- the minimum number of population members that are retained after each such 'survival of the fittest' step (here: 5),
- the number of cg-iterations with no significant improvement of the objective function value after which a population member is marked convergent and not subject to further cg-iterations (here: 80), and
- a difference threshold for two parameter vectors of the deformable model below which they are considered as being equal.

The mentioned parameters have been used in all our experiments. Except for the need of adjusting these parameters, the optimization strategy presented here is a general-purpose method for poorly initialized nonlinear optimization problems and its applicability is not confined to model fitting problems in medical image analysis. Only one example of a *hybrid optimization algorithm* in image analysis is known to us: In [8], a visual reconstruction problem is described mathematically as a coupled (binary-real) nonconvex optimization problem. An informed genetic algorithm is applied to the binary variables, while an incomplete Cholesky

preconditioned cg-method is applied to the remaining real variables for a given configuration of the binary variables visited by the GA. This is different to our approach, where the local and the global part cannot be separated.

5 Experimental Results for 3D Tomographic Images

Scope of experiments In all our experiments, the deformable models were fitted to tip-like and saddle-like anatomical structures and our hybrid optimization algorithm has been compared to purely local cg-optimization w.r.t. to poorly initialized model parameters using

- different *types of image data*: two 3D T1-weighted MR images and a 3D CT image of the human head
- different *types of landmarks*: frontal/occipital horn of the left/right lateral ventricle, left/right zygomatic bone as part of the skull,
- different *fitting measures*: edge distance-based, edge strength-based, and
- different sizes of the *region of interest (ROI)*:
  ROI radius of 10 *vox* and 15 *vox* (*vox*: spatial unit of an image voxel).

Experimental strategy For the different landmarks in the different images, an initial good fit is determined by visual inspection of the fitted deformable model with roughly estimated initial values and by repeating model fittings where necessary. To obtain poor initial estimates for model fitting, the parameter values that result from the initial good fit are varied by adding Gaussian distributed random numbers with zero expectation value and sufficiently large variances. To assess the accuracy of landmark localization, the landmark positions calculated from the fitted deformable models are compared to ground truth positions that were manually determined in agreement with up to four persons (landmark localization error e). In addition, we consider the root-mean-square distance between the edge points of the image and the whole model surface, e_{RMS}, using a Euclidean distance map ([10]) from the image data after applying a 3D edge detection algorithm based on [3]. For each landmark and each image considered, the model fitting algorithm is repeated sufficiently often (here: 100 times) with random model initializations. The mean values and RMS estimates of the resulting values of e, e_{RMS} are tabulated then. For evaluating the gradient ∇g in (2),(3), cubic B-spline interpolation and Gaussian smoothing are used (see [5]).

General results Common to all experiments is that the final objective function value is better by about 10-50% for hybrid optimization than for purely local cg-optimization. In most cases, the landmark localization and the model fitting accuracy also improve significantly. Thus, hybrid optimization turns out to be superior to purely local cg-optimization at the expense of an increase in computational costs of a factor of 5-10 (30s–90s for local cg-optimization and 150s–900s for hybrid optimization on a SUN SPARC Ultra 2 with 300MHz CPU).

The edge distance-based fitting measure in (3) turned out to be more suitable for 3D MR images of the ventricular horns with high signal-to-noise ratio since it incorporates *distance* approximations between the image data and the model surface (*long* range forces, cf. [15]). However, in comparison to (2), it is relatively sensitive to noise. Moreover, it is not suitable for hyperboloids of one sheet due to inaccuracies of the first order distance approximation associated with it.

Results for the ventricular horns The tips of the frontal and occipital horns of the lateral ventricles in both hemispheres are considered here. Typical examples of successful model fitting, which demonstrate the robustness of model fitting and of landmark localization in the case of poorly initialized model parameters, are given in Fig. 2. Here, contours of the model initialization are drawn in black and the results of model fitting using purely local cg-optimization are drawn in grey, while the results of model fitting using the hybrid optimization algorithm are drawn in white. The ground truth landmark positions are indicated by a $\oplus$-symbol. Figs. 2(a),(b) in particular demonstrate the increase of robustness of hybrid optimization in comparison to purely local cg-optimization. As can be seen from the averaged quantitative results in Table 1, hybrid optimization is superior to purely local cg-optimization and yields not only better objective function values, but in most cases also better model fitting (e_{RMS}) and landmark localization (e) results. Note that rather coarsely initialized model parameters have been used ($\overline{e}_{initial} \approx 7 \ldots 9\, vox$), and thus some unsuccessful fitting results – particularly in the case of the less pronounced occipital horns – deteriorate the average accuracy of model fitting as shown in Table 1.

Fitting results for 3D MR images of the horns of the ventricles						
		Model initialization	Edge dist.-b. obj. func.		Edge strength-b. obj. func.	
			local cg-opt.	hybrid opt.	local cg-opt.	hybrid opt.
Frontal horn (left)	e	7.71 ± 3.16	3.28 ± 2.99	1.40 ± 1.18	3.54 ± 2.18	2.49 ± 2.21
	e_{RMS}	2.22 ± 1.10	1.00 ± 0.63	0.65 ± 0.22	1.04 ± 0.31	0.87 ± 0.35
Frontal horn (right)	e	6.57 ± 3.18	3.87 ± 2.16	3.15 ± 2.18	6.55 ± 3.53	5.19 ± 3.70
	e_{RMS}	2.12 ± 1.11	1.05 ± 0.60	0.78 ± 0.25	1.56 ± 1.26	1.28 ± 0.79
Occipital horn (right)	e	9.08 ± 4.42	6.90 ± 3.89	6.68 ± 3.93	4.74 ± 4.33	4.61 ± 4.31
	e_{RMS}	3.00 ± 1.40	2.06 ± 0.93	2.04 ± 0.87	1.34 ± 0.87	1.29 ± 0.78

Table 1. Fitting results averaged over 100 model fittings with randomized poor model initializations for the *frontal/occipital* horns of the lateral ventricles from 3D MR images (e: landmark localization error (in vox), e_{RMS}: RMS distance between deformable model and image data within the region of interest (in vox), $1\, vox = 0.86 \times 0.86 \times 1.2\text{mm}^3$).

Results for the zygomatic bones All results for the zygomatic bones presented here are obtained with the edge strength-based fitting measure (2) from a 3D CT image. Model fitting and landmark localization for the saddle points at the zygomatic bones (e.g., Fig. 2(c)) are not as successful as they are for the tips of the ventricular horns since our geometric primitive, hyperboloids of one sheet, do not describe the anatomical structure at hand as accurate. However, the average landmark localization error e can be reduced from initially $\overline{e}_{initial} = 6.4 \ldots 6.9\, vox$ to $\overline{e} = 2.5 \ldots 3.2\, vox$ and the accuracy of model fitting is $\overline{e}_{RMS} = 1.5 \ldots 1.8\, vox$ ($1 vox = 1.0\text{mm}^3$, interpolated *isotropic* image).

6 Conclusion

In this paper, landmark extraction based on parametric deformable models has been investigated in order to improve the stability of model fitting as well as of landmark localization against poorly initialized model parameters. To this end, a novel hybrid optimization algorithm which can be applied to general nonlinear optimization problems has been introduced and edge strength- and

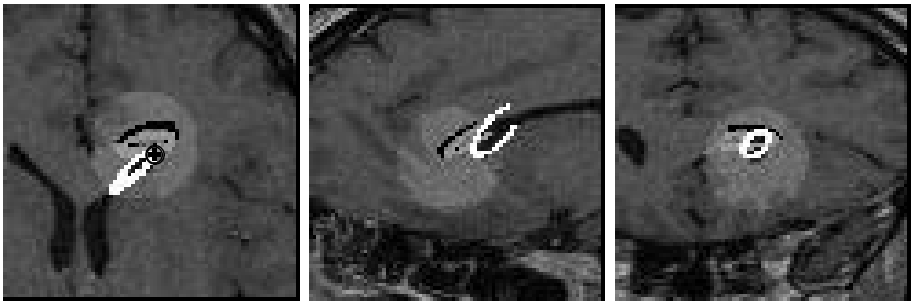

(a) 3D MR image of the *frontal* horn of the *left* lateral ventricle, edge *distance*-based fitting measure, ROI size 15.0 *vox* ($1vox = 0.86 \times 0.86 \times 1.2\text{mm}^3$)

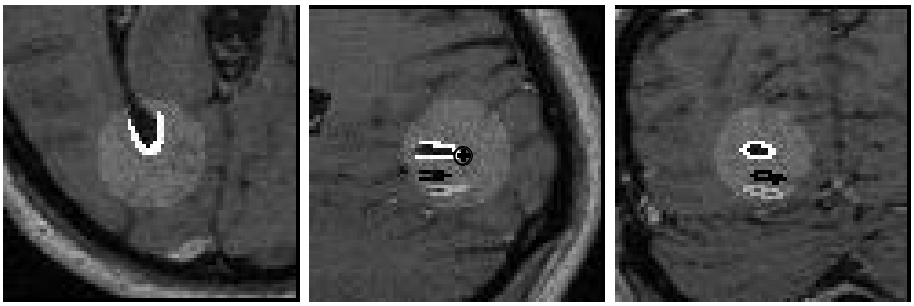

(b) 3D MR image of the *occipital* horn of the *right* lateral ventricle, edge *strength*-based fitting measure, ROI size 15.0 *vox* ($1vox = 0.86 \times 0.86 \times 1.2\text{mm}^3$)

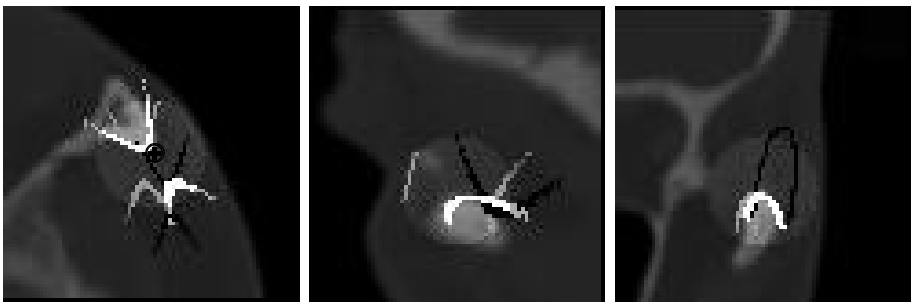

(c) 3D CT image of the *left* zygomatic bone, edge *strength*-based fitting measure, ROI size 15.0 *vox* ($1vox = 0.625 \times 0.625 \times 1.0\text{mm}^3$)

Fig. 2. Examples of successfully fitting tapered and bended half-ellipsoids to 3D MR images of the frontal and occipital horns of the lateral ventricles (Fig. 2(a-b)) as well as of fitting a half-hyperboloid with no further deformations to a 3D CT image of the zygomatic bone (Fig. 2(c)). Contours of the model surfaces in axial, sagittal, and coronal planes are depicted here (from left to right). *Black*: model initialization, *grey*: fitting result for local cg-optimization, and *white*: fitting result for our hybrid optimization algorithm. The ground truth landmark positions are indicated by a $\oplus$-sign here.

edge distance-based fitting measures have been compared. Experimental results demonstrate the applicability of our hybrid optimization algorithm as well as the increased robustness in the case of poorly initialized parameters as compared to purely local cg-optimization. However, the experimental results do not clearly favour one fitting measure. For the frontal horns of the lateral ventricles, our edge distance-based fitting measure yields a more successful model fitting, while for the less pronounced occipital horns of the lateral ventricles and for the zygomatic bones, the edge strength-based fitting measure is more suitable.

References

1. E. Bardinet, L.D. Cohen, and N. Ayache. Superquadrics and Free-Form Deformations: A Global Model to Fit and Track 3D Medical Data. *Proc. CVRMed'95*, LNCS 905, pp. 319–326. Springer, 1995.
2. R. Bertolini and G. Leutert. *Atlas der Anatomie des Menschen. Band 3: Kopf, Hals, Gehirn, Rückenmark und Sinnesorgane.* Springer, 1982.
3. J.F. Canny. A Computational Approach to Edge Detection. *PAMI*, 8(6):679–698, 1986.
4. K. Delibasis and P.E. Undrill. Anatomical object recognition using deformable geometric models. *Image and Vision Computing*, 12(7):423–433, 1994.
5. S. Frantz, K. Rohr, and H.S. Stiehl. Localization of 3D Anatomical Point Landmarks in 3D Tomographic Images Using Deformable Models. *Proc. MICCAI2000*, LNCS 1935, pp. 492–501. Springer, 2000.
6. G.H. Golub and C.F. Van Loan. *Matrix Computations.* Johns Hopkins University Press, 1996.
7. D. Goldberg. Genetic Algorithms in Search, Optimization and Machine Learning. Addison Wesley, 1989.
8. S.H. Lai and B.C. Vemuri. Efficient hybrid-search for visual reconstruction problems. *Image and Vision Computing*, 17(1):37–49, 1999.
9. T. McInerney and D. Terzopoulos. Deformable Models in Medical Image Analysis: A Survey. *Medical Image Analysis*, 1(2):91–108, 1996.
10. D.W. Paglieroni. A Unified Distance Transform Algorithm and Architecture. *Machine Vision and Applications*, 5(1):47–55, 1992.
11. K. Rohr. On 3D differential operators for detecting point landmarks. *Image and Vision Computing*, 15(3):219–233, 1997.
12. J. Sobotta. *Atlas der Anatomie des Menschen. Band 1: Kopf, Hals, obere Extremität, Haut.* Urban & Schwarzenberg, 19th edition, 1988.
13. F. Solina and R. Bajcsy. Recovery of Parametric Models from Range Images: the Case for Superquadrics with Global Deformations. *PAMI*, 12(2):131–147, 1990.
14. L.H. Staib and J.S. Duncan. Model-Based Deformable Surface Finding for Medical Images. *IEEE Trans. Med. Imag.*, 15(5):720–731, 1996.
15. D. Terzopoulos and D. Metaxas. Dynamic 3D Models with Local and Global Deformations: Deformable Superquadrics. *PAMI*, 13(7):703–714, 1991.
16. J.-P. Thirion. New Feature Points based on Geometric Invariants for 3D Image Registration. *Internat. Journal of Computer Vision*, 18(2):121–137, 1996.
17. V. Vaerman, G. Menegaz, and J.-P. Thiran. A Parametric Hybrid Model used for Multidimensional Object Representation. *Proc. ICIP'99*, vol. 1, pp. 163–167, 1999.
18. B.C. Vemuri and A. Radisavljevic. Multiresolution Stochastic Hybrid Shape Models with Fractal Priors. *ACM Trans. on Graphics*, 13(2):177–207, 1994.
19. Z. Zhang. Parameter Estimation Techniques: A Tutorial with Application to Conic Fitting. *INRIA Rapport de recherche*, No. 2676, 1995.